Journal of Ceramic Processing Research. Vol. 4, No. 2, pp. 49~55 (2003)

J O U R N A L O F
Ceramic Processing Research

Computer modeling of a multi-run growth technique for sapphire ribbons

A.V. Borodin*, V.A. Borodin[a], A.V. Zhdanov[b] and I.S. Petkov[c]
Experimental Factory of Scientific engineering (EZAN RAS) 142432, Chernogolovka, Moscow region, Russia
[a]Experimental Factory of Scientific Engineering (EZAN RAS)
[b]Institute of Solid State Physics (ISSP RAS)
[c]ROSTOX-N Ltd. 142432, Chernogolovka, Moscow region, Russia

Multi-run growth is most commonly applied to provide a high yield of shaped crystals. The presence of several crystals in a melting zone and a radiative heat exchange between them pose difficulties in the optimization of the heat zone design and growth conditions. The trial-and-error experiments can hardly be applied because of high cost in terms of materials and time. Moreover, the presence of many parameters under consideration and their interaction make a tentative search a very arduous task. In this paper, the multi-run growth process for sapphire ribbons is studied on the basis of mathematical modeling and the optimized relationships are found.

Key words: Moedling, EFG, Multi-run growth, Sapphire.

Introduction

The EFG (edge-defined fed film growth) simultaneous growth technology essentially increases the process productivity, lowers power and water consumption, and finally cuts down the costs of EFG crystals. At the same time, multi-run growth requires a fine adjustment of the thermal field inside a heat zone and an optimum design of a die assembly. In this paper the simultaneous growth process of sapphire ribbons is studied on the basis of mathematical modeling. It is supposed, that there is a radiative heat exchange between the lateral diffuse-gray surfaces of ribbons. The two dimensional model of the growth process includes Stokes and diffusion equations, the Stephan problem, and an equation for a stress function. All of the problems are solved by a finite element method [1-3].

The final goal of finite element analysis is to define the set of process variables which will simultaneously (if possible) minimize the following:

1) the difference in temperature distribution of packed ribbons to ensure growth control by heating power variations;

2) the magnitude of thermal stress in each ribbon of the package to prevent block formation;

3) the magnitude of impurity concentration at local regions of the interface near the lateral surface as an impurity oversaturation in these regions sets preferable conditions for bubble generation as a new phase and their further growth.

The solution method of the whole problem is based on the sequence of iterative procedures. It is convenient to find a temperature field in an individual ribbon assuming that there is only radiative heat exchange between its lateral surfaces and an ambient and then use this temperature map as the initial temperatures in the rest of the ribbons involved in radiation exchange.

The Stefan-type problem of phase transition includes in itself heat transfer and Stokes equations and their boundary conditions, and consists of finding temperatures for liquid and solid phases, melt velocities in the meniscus, the shape of the interface boundary, the profile curve of the meniscus and, finally, the thickness of the growing ribbon.

Then the ribbon is multiplied into an array of identical crystals. The surfaces of adjacent ribbons, the openings between their upper ends, and the gaps between sub-dies form the enclosures. Now the problem of the radiative heat exchange between lateral diffuse-grey surfaces of any adjacent ribbons is formulated by requiring a balance between surface temperatures and their radiation fluxes [4]. Its solution yields a new ambient temperature distribution in each of the enclosures. Then the procedures of step one, except multiplying, are applied for all of the crystals, and new temperature maps and therefore temperature distributions of lateral surfaces are found. The surfaces with recent distributions exchange radiation on the next loop of the computational cycle. This procedure is performed until the temperature change in each ribbon is less than a preset convergence factor.

*Corresponding author:
Tel : 007 (095) 913-21-08, 962-80-50
Fax: 007 (096-52) 4-95-88
E-mail: borodin@ezan.ac.ru

In the final stage the problems of a thermoelasticity and an impurity distribution should be solved.

Model Formulation

From the beginning we shall take into account the fact that the heat transfer problem needs to be formulated individually for all the inner ribbons of the package and the two outer ribbons. This distinction originates from the difference of thermal exchange between the lateral surfaces of adjacent inner ribbons and these of the two outer ribbons with the neighboring medium.

A diagram of the crystallization process and the choice of the coordinate system are illustrated in Fig. 1. Indices 1 and 2 denote the quantities referring to the melt and crystal, respectively. The distribution of temperature in the regions D_1 and D_2 involving the melt in the meniscus and the crystal, is described by the thermal conduction equation:

$$\Delta T_i - \zeta_i(V_i, \Delta T_i) = 0, \ (x,y) \in D_i, \ \zeta_i = \frac{\rho_i c_i}{k_i}, \ i = 1,2, \qquad (1)$$

where $V_1=(u_1, v_1)$ is the field of the melt velocities in the meniscus and $V_2=(0, V_0)$ is the rate of pulling.

At the interface $H(x)$, the Stefan condition should be fulfilled:

$$k_2(n, \nabla T_2) - k_1(n, \nabla T_1) = \rho_2 V_0 \Delta H_f (1 + H_x'^2)^{1/2}, \qquad (2)$$

$$T_1[x, H(x)] = T_2[x, H(x)] = T_m, \ -h_1 \le x \le h_2, \ y = H(x). \qquad (3)$$

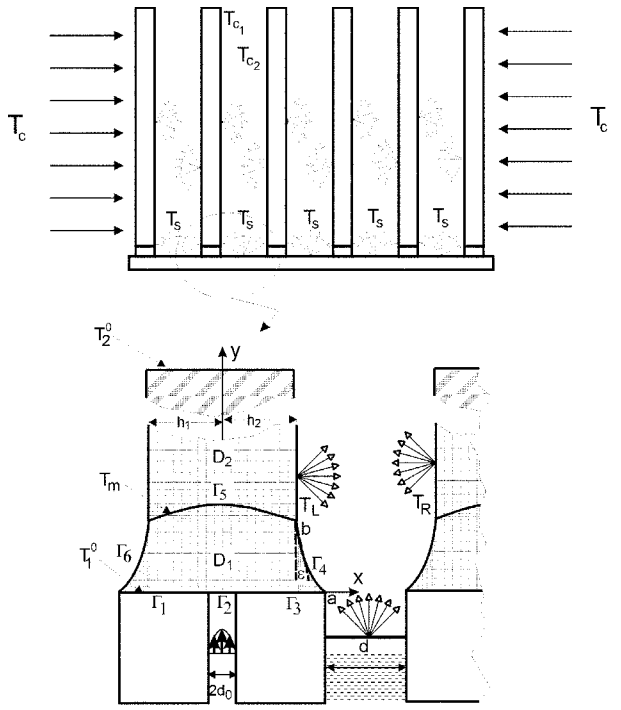

Fig. 1. The scheme of multi-run growth, coordinate system, and labels used.

For the two lateral surfaces of the outer ribbons heat transfer from the melt and the crystal to the ambient at temperature $T_c(y)$, which depends only on the height, is accomplished by convection and radiation:

$$-k_i \frac{\partial T_i}{\partial \vec{n}} = h_{Gi}(T_i - T_c) + \sigma \varepsilon_i (T_i^4 - T_c^4), \qquad (5)$$

and the equations describing radiative heat exchange between the lateral surfaces of adjacent inner ribbons will be derived below.

In addition, at the die top face and at the top of the crystal the following temperatures are preset:

$$T_1(x,0) = T_1^0(x), \ -a \le x \le a, \ T_2(x,l) = T_2^0(x), \ -h_1 \le x \le h_2. \qquad (6)$$

The right-hand profile curve of meniscus $f(y)$ satisfies the Laplace equation and the boundary conditions:

$$\rho_2 g(y + H_{eff}) = \sigma_{LG} \frac{d}{dy}\left[\frac{df/dy}{(1 + (df/dy)^2)^{1/2}}\right], \qquad (7)$$

$$f(0) = a, \quad -\left.\frac{df}{dy}\right|_{y=H(h_2)} = tg\varepsilon_0 . \qquad (8)$$

A similar equation describes the other curve. Both equations have the same value of H_{eff}.

The velocity field in the melt $V_1=(u_1, v_1)$ satisfies Stokes equations:

$$\mu \Delta V_1 + \rho_1 (V_1, \nabla) V_1 = \nabla P + F, \ V_{1n} = 0,$$
$$div V_1 = 0. \qquad (10)$$

The boundary of overall area D_1 consists of 6 sections (G_i, $i=1, .., 6$) on which, in accordance with melt flow conditions, the boundary data are given.

At the interface $y=H(x)$, for boundary Γ_2, we have

$$V_{1n} = V_0[1 + (H_x')^2]^{1/2}, \quad V_{1\tau} = 0. \qquad (11)$$

At the boundaries Γ_4 and Γ_6 that appropriate to the melt free surface, the normal component of the velocity tends to zero, and besides the tangent strain tends to zero:

$$V_{1n} = 0, \ [(\vec{\tau}, DV_1), \vec{n}] = 0, \quad x = f(y). \qquad (12)$$

And the boundaries Γ_1, Γ_3, Γ_2, that correspond to the die top face and to the outlet of a capillary gap, satisfy the following:

$$u_1 = 0, \ v_1 = 0, \ (x,y) \in \Gamma_1 \cup \Gamma_3, \ u_1 = 0,$$
$$v_1 = AV_0\left[1 - \left(\frac{x}{d_0}\right)^2\right], \ (x,y) \in \Gamma_2 \qquad (14)$$

The lateral surfaces of all ribbons we consider to be diffuse – grey. This means that a part of an incident

radiative flux $q_{i,k}(r_k)$ is mirrored evenly in all directions by a lateral surface of a ribbon. The resultant radiative flux $q_k(r_k)$ for the surface area with a position vector r_k is given by

$$q_k(r_k)=q_{0,k}(r_k)-q_{i,k}(r_k),\ k=1,2, \tag{15}$$

here the indices 1 and 2 denote the surfaces of any adjacent ribbons facing each other.

In the case of radiative heat exchange between two parallel diffuse-gray surfaces the effective radiative flux $q_{0,k}(r_k)$ is the sum of self radiation and reflected radiation fluxes and fits a system of integral equations [4]:

$$q_{0,k}(r_k)=\varepsilon_k\sigma T_k^4(r_k)+(1-\varepsilon_k)q_{i,k}(r_k) \tag{16}$$

$$q_{0,1}(y)-(1-\varepsilon)\frac{1}{2}\int_0^L q_{0,2}(x)\frac{b^2}{[(x-y)^2+b^2]}dx = \sigma(\varepsilon T_1^4(y)+(1-\varepsilon)T_R^4) \tag{17}$$

$$q_{0,2}(y)-(1-\varepsilon)\frac{1}{2}\int_0^L q_{0,1}(x)\frac{b^2}{[(x-y)^2+b^2]}dx = \sigma(\varepsilon T_2^4(y)+(1-\varepsilon)T_R^4) \tag{18}$$

where $T_R^4=T_S^4\cdot\frac{1}{2}\left[1-\frac{y}{\sqrt{y^2+b^2}}\right]$, $b=d+2a-h_1^{(2)}-h_2^{(2)}$, see Fig. 1.

This system ones solved provides us with the values of $q_{0,1}$ and $q_{0,2}$. In the next step we find the incident radiative flux $q_{i,k}(r_k)$ using equations (15), (16).

Here we introduce the concept of the ambient temperature due to the radiative heat exchange between neighboring lateral surfaces:

$$T_{ck}=\sqrt[4]{q_{i,k}/\sigma},\ i=1,2, \tag{19}$$

Thus, for all inner ribbons the law of heat transfer thermal exchange will be described by the formula (5) if to put $T_c=T_{ck}$.

The stress function F is introduced by the formulae

$$\sigma_x=\frac{\partial^2 F}{\partial y^2},\ \sigma_y=\frac{\partial^2 F}{\partial x^2},\ \sigma_{xy}=\frac{\partial^2 F}{\partial x\partial y}. \tag{20}$$

In the case of a plain strain state, F satisfies the relation:

$$\Delta^2 F=-\frac{E}{1-\nu}\alpha_t\Delta T_2,\quad (x,y)\in D_2. \tag{21}$$

The boundary conditions for F are found by requiring that there are no surface forces:

$$F=0,\ \frac{\partial F}{\partial n}=0. \tag{22}$$

The impurity concentration in a melt is described by the equation

$$D\Delta C-\vec{V}\nabla C=0 \tag{23}$$

and the boundary conditions:

$$\frac{\partial C}{\partial y}=0,\ (x,y)\in\Gamma_1\cup\Gamma_3, \tag{24}$$

$$C=C_1,\ (x,y)\in\Gamma_2, \tag{25}$$

$$\frac{\partial C}{\partial\vec{n}}=0,\ (x,y)\in\Gamma_4\cup\Gamma_6, \tag{26}$$

$$-D\frac{\partial C}{\partial\vec{n}}=V_0(k_0-1),\ (x,y)\in\Gamma_5. \tag{27}$$

The solution of this problem by the finite element method is given in [5, 6].

Numerical Analysis Results

The multiple growth of six sapphire ribbons is investigated. The initial input data is taken in compliance with experimentally measured temperatures and the features of a thermal unit design. So, in particular, all sub-dies top face temperatures in the die assembly and the melt temperature at each capillary outlet are uniform, the value of seed crystal temperature is reduced in accordance with the length pulled, and an ambient temperature drop is set to be linear with the distance above the die assembly.

Table 1 shows input values for different runs of simulation software. The temperature fields, interface shapes and positions in all 6 ribbons for the input data (A) are given in Fig. 2. The results exhibit significant differences between temperature distributions, meniscus

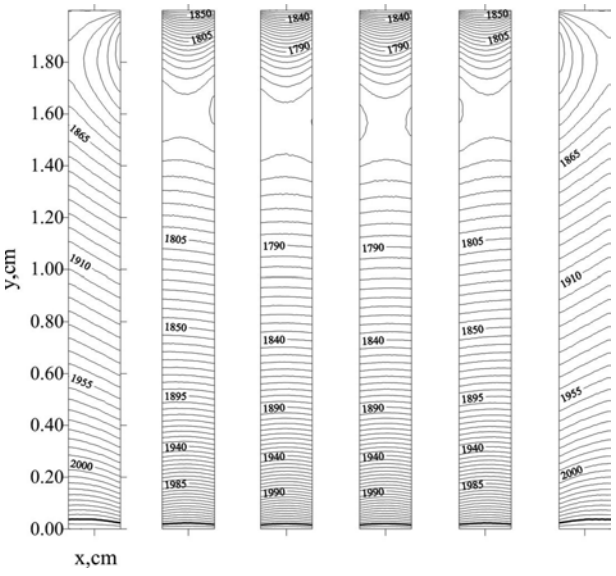

Fig. 2. Temperature distributions in ribbons and positions of crystallization fronts.

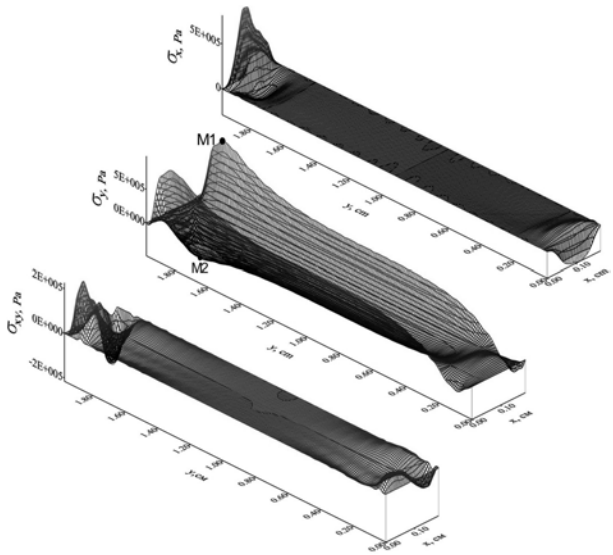

Fig. 3. Typical thermoelastic fields in the outer ribbon of the packet.

heights and interface shapes of the outer and the inner ribbons. This fact is referred to as a radiative shielding effect of the outer ribbons.

Figure 3 shows the surface of normal σ_x, σ_y, and tangent σ_{xy} stresses determined over the calculated region of the right outer ribbon. It is seen that the stresses are concentrated at the crystallization front and lateral face of the ribbon. The normal stress, σ_x is a maximum near the center of the ribbon in the crystallization front (there is some displacement of the maximum to the ribbon lateral face due to asymmetry of the thermal field) and drops drastically towards the upper end of the crystal. The normal stress, σ_y reaches its maximum on the lateral surface near the crystallization front and decreases gradually with crystal length. The tangential stress is a maximum at some distance from the front, and its magnitude is approximately seven times smaller than that of the normal stresses. In general, the stress magnitude and exact location of its maximum points are found to depend on ambient temperature, the length of crystals, the position of a certain ribbon, the temperature of the die top face, the gap between adjacent sub-dies, etc.

The change of the forms and positions of the crystallization fronts were studied as a function of pulling rate and the gap between adjacent sub-dies. The results are introduced by Fig. 4(a, b, c) (in view of the problem symmetry only the left half is shown). Here (and later) labels 1, 2, and 3 will denote the first, the second, and the third ribbon counted left to right. Figure 4(a) demonstrates that a pulling rate decrease (Input (F), Table 1) produces a diminution of heights of all menisci. This modification is almost identical for all of the ribbons. So, a pilling rate variation is unable to level the temperature distributions in different ribbons. A lessening of the gap between adjacent sub-dies (to put it differently: “clearance”) (Input (B)) produces a these desirable leveling of temperature distributions. These relationships are clearly seen in Fig. 4(a, b) which presents the thickness of the ribbons as a function of the pulling rate (a) and clearance (b): the difference in thickness disappear with a clearance decrease. The same study, performed for a lower initial ambient temperature (Input (C)), gives similar dependences.

For further analysis, which involves goals 1, 2 and

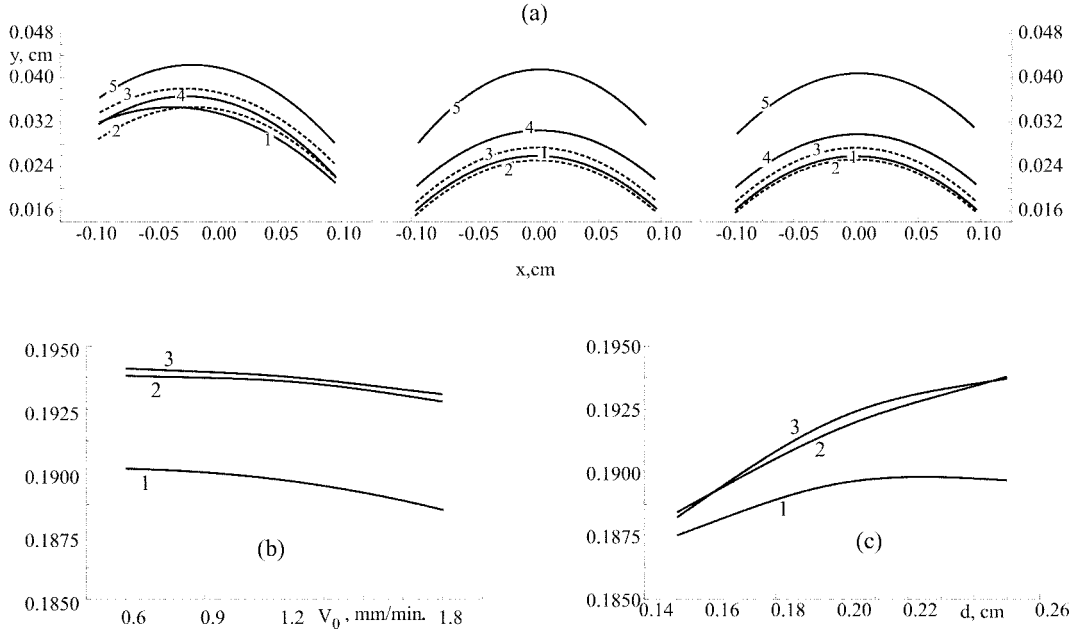

Fig. 4. Position and shape changes of crystallization fronts as a function of the pulling rate and the gap between sub-dies. 1-V0=1.2 mm/minute, d=0.25 mm; 2-V0=0.6 mm/minute, d=0.25 mm; 3-V0=1.8 mm/minute, d=0.25 mm; 4-V0=1.2 mm/minute, d=0.20 mm; 5-V0=mm/minute, d=0.15 mm.

Table 1.

Input parameters	(A)	(B)	(C)	(D)	(E)	(F)
T_1^0, °C	2060	2060	2060	2053, 2055, 2060	2060	2060
L, cm	1, 2, 3, 4, 5, 6, 7, 8	5	5	5	5	5
T_2^0, °C	$T_1^0-100^{°C/cm}\times L$	1560	1560	$T_1^0-100^{°C/cm}\times L$	1560	1560
T_c^0, °C	2030	2030	1850	2030	2030	2030
t_d, °C/cm	70	70	70	70	70	70
V_0, cm/minute	0.12	0.12	0.12	0.12	0.12	0.18, 0.12, 0.08
d, cm	0.25	0.35, 0.25, 0.20, 0.15	0.35, 0.25, 0.20, 0.15	0.25	0.25	0.25
$2d_0$, cm	0.06	0.06	0.06	0.06	0.06, 0.04, 0.03	0.06
$2a$, cm	0.2	0.2	0.2	0.2	0.2	0.2

then 3 (see the Introduction), we use the verification strategy checking if the relationship obtained satisfies the rest of the minimization criteria, and we vary some other parameter if it does not.

For the analysis of thermal stress behavior it is convenient to operate with maximal (positive) and minimal (negative) values of the corresponding stress surfaces (points M_1 and M_2, Fig. 4).

Figure 5(a) presents the dependence of extremal stress values with pulled length (Input (A)). The ribbons are strongly stressed when shortest, the maximal values are located in the inner crystals and a stress leveling effect is observed as a crystal length increase. Figure 5(b) shows thermal stresses in ribbons plotted as a function of the value of the gap between adjacent sub-dies. For the case of hot surroundings of the die

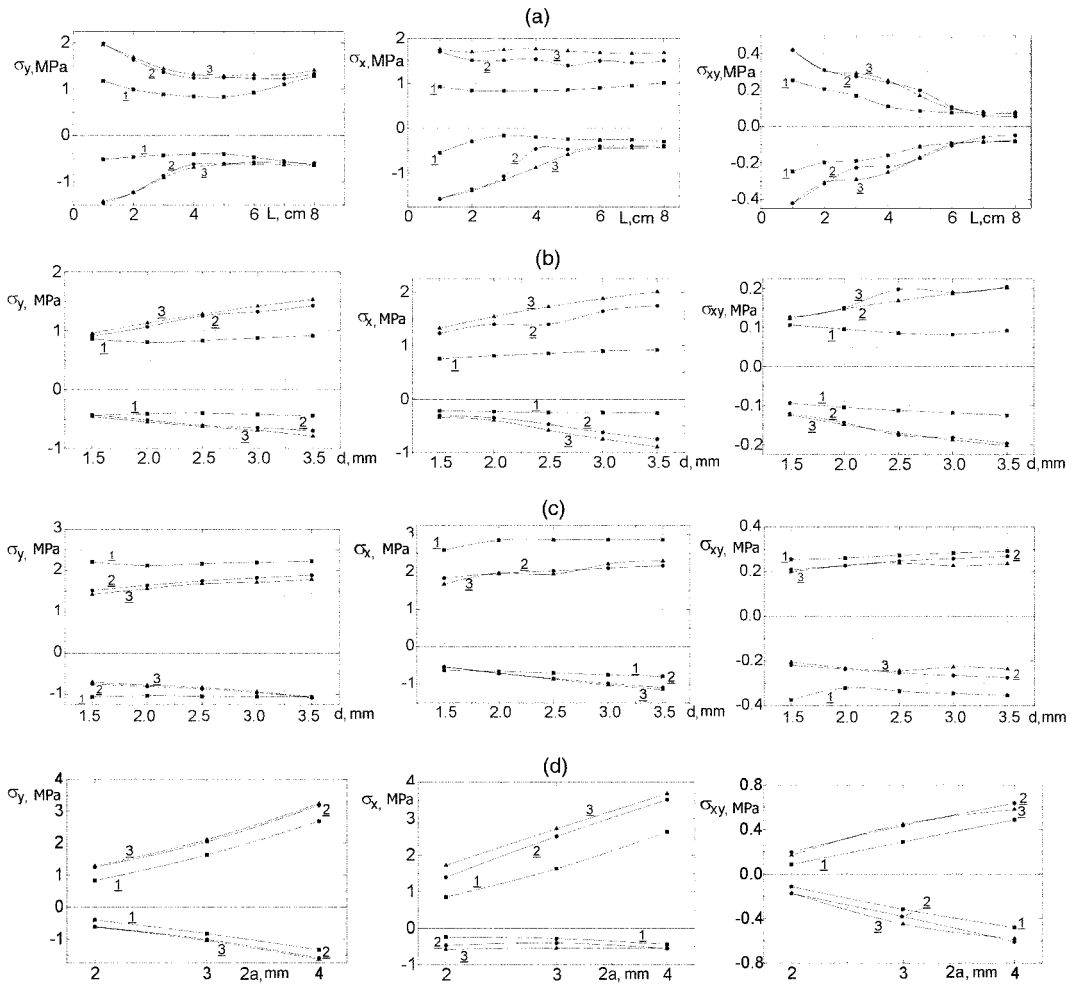

Fig. 5. The extremal stresses change with pulled length (a), as a function of the gap between sub-dies (b), (c), and as a function of sub-die thickness (d).

shown above levels the temperature distributions of the ribbons, also causes stresses to fall in all crystals of the package. The results of the same study, performed for a lower initial ambient temperature (Input (C)), demonstrate rather a poor effect of stress reduction, besides magnitude of the stress in the crystals is significantly higher, Fig. 5(c). So, we can preliminary conclude that an increase of ambient initial temperature jointly with a decrease in the gap between adjacent sub-dies minimizes the difference in temperature distributions and reduces magnitude of the thermal stress in multi-run ribbons.

As so far the best growth conditions (at least two minimization criteria are satisfied) are achieved for the input set (B) with a small clearance between adjacent sub-dies, we use this system for a further study to analyze the influence of die top face temperature and of die capillary width on temperature distributions and stress behavior (inputs (D) and (E)). The calculations performed for the input (D) revealed that a die top temperature drop from 2060°C to 2055°C gave a sharp rise in the normal stress σ_x in all crystals of the package (for example, the maximal stress in the outer ribbon rises from 0.8 to 1.2 MPa), while the values of σ_y and σ_{xy} are nearly constant. There was no noticeable effect in the leveling of the temperature distributions with die top temperature variation. The decrease of the sub-die capillary from 0.6 to 0.3 mm (input (E)) also did not produce a desirable effect on the temperature distributions and stress magnitude.

Finally, the influence of sub-dies compacting, their capillary width, and top face temperature on the impurity distribution in the liquid menisci of ribbons were analyzed (Inputs (B) and (E)). The surface of a typical impurity distribution in a liquid meniscus of the outer ribbon is shown in Fig. 6. The concentration reaches its maximums at the crystallization front at a distance of 25-45 micrometres from the meniscus profile curves. The dependences of impurity concentration at the crystallization front in terms of the parameters mentioned above are given in Fig. 7(a, b). It may be noted that for all considered conditions of growth the concentration in the meniscus of the second ribbon is much higher than that in the rest of the menisci. We conclude that this can be referred to a greater deflection of the crystallization front in the second ribbon. Thankfully the results presented in Fig. 7(a) demonstrate that sub-dies compaction helps to reduce impurity concentration. The same effect is achieved via widening of capillary the gap, Fig. 7(b). The drop of die top temperature from 2055°C to 2053°C on the contrary causes segregation of impurities in the corners of the menisci, Fig. 7(c).

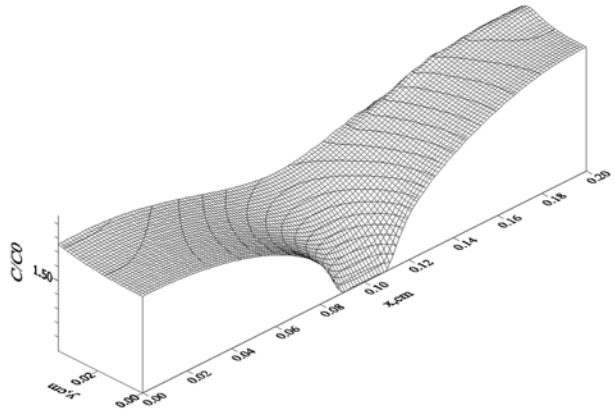

Fig. 6. The surface of typical impurity concentration.

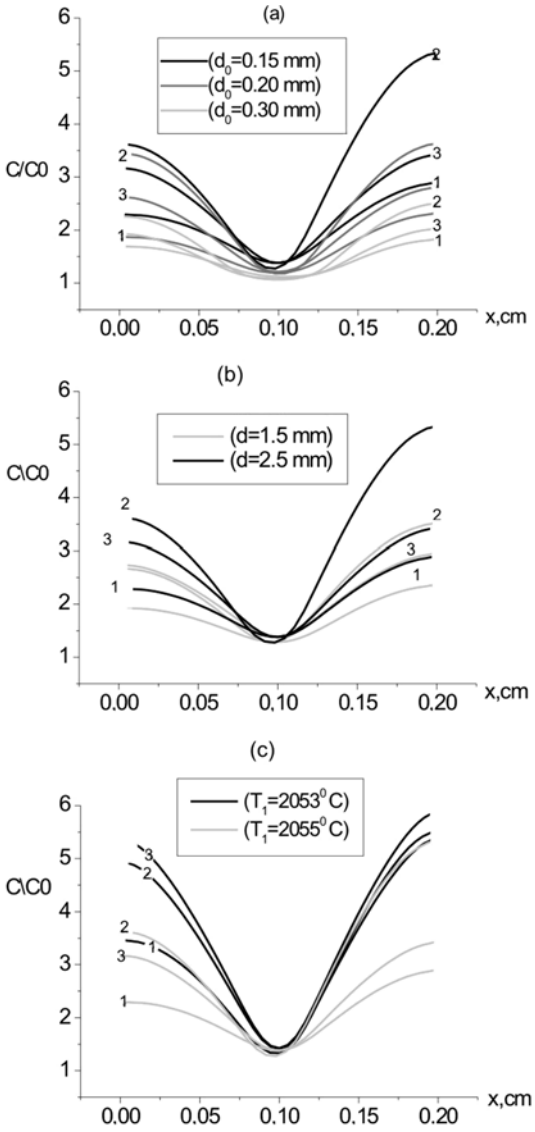

Fig. 7. Impurity distribution at the crystallization fronts as a function of (a) capillary gap width, (b) width of the gap between sub-dies, (c) die top face temperature.

Conclusions

In this paper, a mathematical model and computational algorithm for calculation of temperature distributions in multi-run sapphire ribbons were developed. To this

model were added the problems of thermoelasticity and impurity concentration. On the basis of modeling the simultaneous growth process was studied under variations of technological parameters to find the optimized ones. It was established that a decrease of the gap between adjacent sub-dies jointly with an increase of ambient initial temperature minimizes the difference in temperature distributions, reduces the thermal stress and impurity concentration. The difference in temperature distribution between the inner and outer ribbons can be further diminished by using radiation shields that emulate outer ribbons. The die top face temperature should not be allowed to drop down much as there is a sharp growth of normal stress and impurity concentration in this case. This drop may be checked indirectly by observing menisci heights or via weight signal monitoring. The hot ambient near die assembly, which as shown above decreases the stress magnitude and enhances the favorable effect of sub-dies compacting, can be achieved by lowering the die assembly deeper into a heater. And finally, the reasonable choice of die capillary width helps to lower impurity concentration.

Nomenclature

k_i : Thermal conductivity
ρ_i : Densities of the melt (i=1) and of the crystal (i=2)
σ_{LG} : Melt-gas surface tension
σ : Stefan-Boltzmann constant
h_G : Heat transfer coefficient
ε : Emissivity of the crystal lateral surface
ΔH_f : Heat of fusion
α_t : Thermal expansion coefficient
c_i : Heat capacity
E : Young's modulus
ν : Poisson's coefficient
F : Stress function
$\sigma_x,\sigma_y,\sigma_{xy}$: Normal and tangential stresses
μ : Melt dynamic viscosity
D : Diffusion coefficient
C : Concentration in meniscus
C_0 : Concentration at capillary gap outlet
k_0 : Impurity distribution coefficient
V_0 : Crystal pulling rate
V_1 : Melt flow velocity
$V_{1n},V_{1\tau}$: Normal and tangential components of melt flow velocity
$\boldsymbol{n}$: Normal vector to an any boundary
τ : Tangential vector to an any boundary
$f(y)$: Profile curve of meniscus
T_m : Melting temperature
T_1^0 : Temperature at die surface
T_2^0 : Temperature at crystal upper ends
T_c : Ambient temperature
t_d : Ambient temperature drop
q_k : Resultant radiation flux
$q_{i,k}$: Incident radiation flux
$q_{0,k}$: Effective radiation flux
g : Acceleration due to gravity
Γ_i : Boundaries of meniscus region
a : Die half dimension
d_0 : Capillary gap half dimension
d : Gap between adjacent sub-dies
L : Crystal length
ε_0 : Angle of growth
H_{eff} : Height of die edges above melt pool
h_1,h_2 : Distance from die symmetry line to left and right lateral crystal surfaces
Def V_1 : Deformation rate tensor

References

1. C.A.J. Eletcher, Computational Galerkin Methods (Springer, New York, Berlin, Heidelberg, Tokio, 1984).
2. A.R. Mitchell and R. Wait, The Finite-Element Method in Partial Differential Equations (Wiley, Chichester, New York, Brisbane, Toronto, 1977).
3. G. Strang and G.J. Fix, An Analysis of the Finite Element Method (Prentice-Hall, Englewood Cliffs, NJ, 1973).
4. R. Zigel and J. Howell, Thermal Heat Transfer by Radiation (Moscow, 1975)
5. A.V. Borodin, *et al*., Izv. RAN. Ser. Phys. 9 (1999) 1719-1731.
6. A.V. Borodin, PhD Dissertation, Moscow Institute of Steel and Alloys (Technological University) (2000).